pubs.acs.org/acschemicalbiology

Letters

Fluorescent D-Amino Acids for Super-resolution Microscopy of the Bacterial Cell Wall

Chen Zhang, Luc Reymond, Ophélie Rutschmann, Mischa A. Meyer, Julien Denereaz, Jiangtao Qiao, Faustine Ryckebusch, Juliette Griffié, Willi L. Stepp, and Suliana Manley*

Cite This: *ACS Chem. Biol.* 2022, 17, 2418–2424

Read Online

ACCESS | Metrics & More | Article Recommendations | Supporting Information

ABSTRACT: Fluorescent D-amino acids (FDAAs) have previously been developed to enable *in situ* highlighting of locations of bacterial cell wall growth. Most bacterial cells lie at the edge of the diffraction limit of visible light; thus, resolving the precise details of peptidoglycan (PG) biosynthesis requires super-resolution microscopy after probe incorporation. Single molecule localization microscopy (SMLM) has stringent requirements on the fluorophore photophysical properties and therefore has remained challenging in this context. Here, we report the synthesis and characterization of new FDAAs compatible with one-step labeling and SMLM imaging. We demonstrate the incorporation of our probes and their utility for visualizing PG at the nanoscale in Gram-negative, Gram-positive, and mycobacteria species. This improved FDAA toolkit will endow researchers with a nanoscale perspective on the spatial distribution of PG biosynthesis for a broad range of bacterial species.

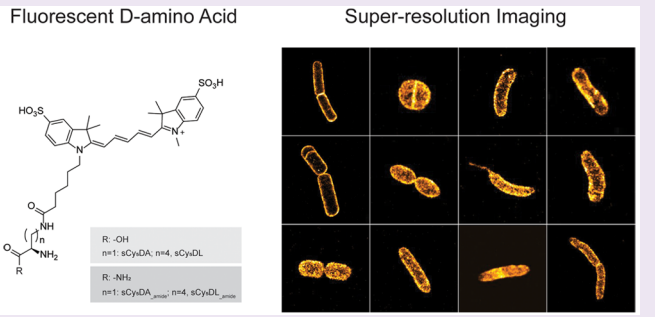

Peptidoglycan (PG) is the essential material that composes the bacterial cell wall. Surrounding the cytoplasmic membrane, PG forms a mesh-like structure from long glycan chains that are cross-linked by D-amino acid (DAA)-containing short peptides, thus providing mechanical rigidity and protecting cells from external stresses. PG biosynthesis is crucial for adapting the bacterial cell shape as cells grow, and its exclusivity as a biomolecule found in bacteria makes it a valuable target for novel antibiotics. To investigate the role of PG in bacterial growth and survival, fluorescent D-amino acids (FDAAs) were developed by conjugating fluorophores with DAA backbones.[1,2] FDAAs can incorporate into PG cross-links by transpeptidase-mediated reactions.[3] Specifically, FDAAs replace the fourth or fifth DAA of the PG stem peptide, which is further cross-linked through the activity of periplasmic D,D-transpeptidases (and L,D-transpeptidases if present).[3] Therefore, FDAAs can enable visualization of nascent PG biosynthesis in living cells. In the intervening years, additional FDAAs have been synthesized and reported; for example, FDAAs with distinct fluorescence spectra,[4] and fluorogenic FDAAs that become fluorescent only upon incorporation into the cell wall.[5] These tools allow researchers to resolve the history of PG biosynthesis in individual cells via a multistep pulse labeling, or real-time continuous tracking of PG biosynthesis with high temporal resolution.

Despite the insights already gained through the use of FDAAs, bacterial cells often lie at the diffraction limit of light microscopy (~250−400 nm), and PG ultrastructure is thus challenging to observe. Super-resolution optical microscopy methods allow fluorescence imaging with a resolution beyond the diffraction limit.[6] Among them, structured illumination microscopy (SIM), which does not require specific photophysical properties of fluorophores themselves and achieves a resolution of ~120 nm, has been widely applied to study FDAA-labeled nascent PG.[7−9] Another super-resolution method, SMLM (also referred to as PALM or STORM), provides a much higher spatial resolution (~30 nm) and relies on nonlinear optical transitions of the fluorophores. In brief, transitions between fluorescent and dark states result in single molecule photoblinking, which when optimized enables the emission from each fluorophore to be temporally and spatially isolated from its neighbors. By localizing single emitter events from thousands of imaging frames, one can reconstruct a SMLM image.[10] Given the unusual properties required of fluorophores for SMLM, few studies have reported its use in conjunction with FDAAs. Two strategies have been applied to FDAAs in SMLM imaging: (1) to synthesize an FDAA incorporating a fluorophore; (2) to synthesize a DAA derivative that can be modified via a "click reaction". In the first case, the FDAAs TAMRA-D-lysine (TDL) and Cy_3B-D-

Received: June 10, 2022
Accepted: August 15, 2022
Published: August 22, 2022

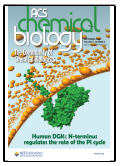

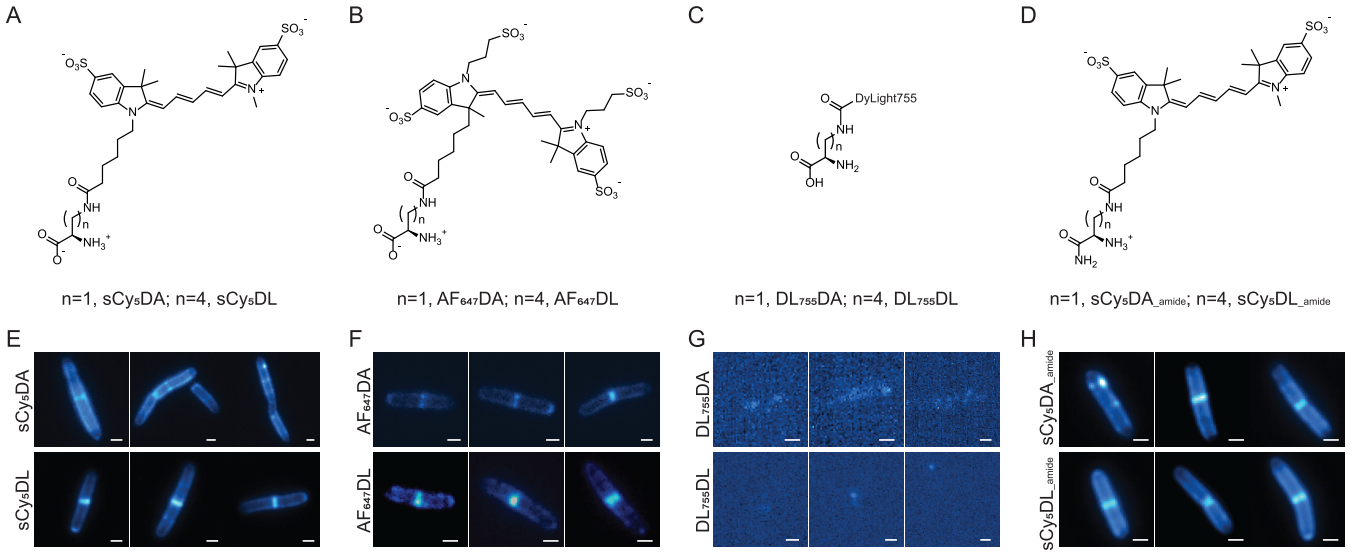

Figure 1. Newly synthesized FDAAs (A–D). Examples of corresponding widefield images of FDAA-labeled *B. subtilis* cells (E–H) after 20 min incubation with 0.5 mM during midexponential phase. Scale bar: 1 μm.

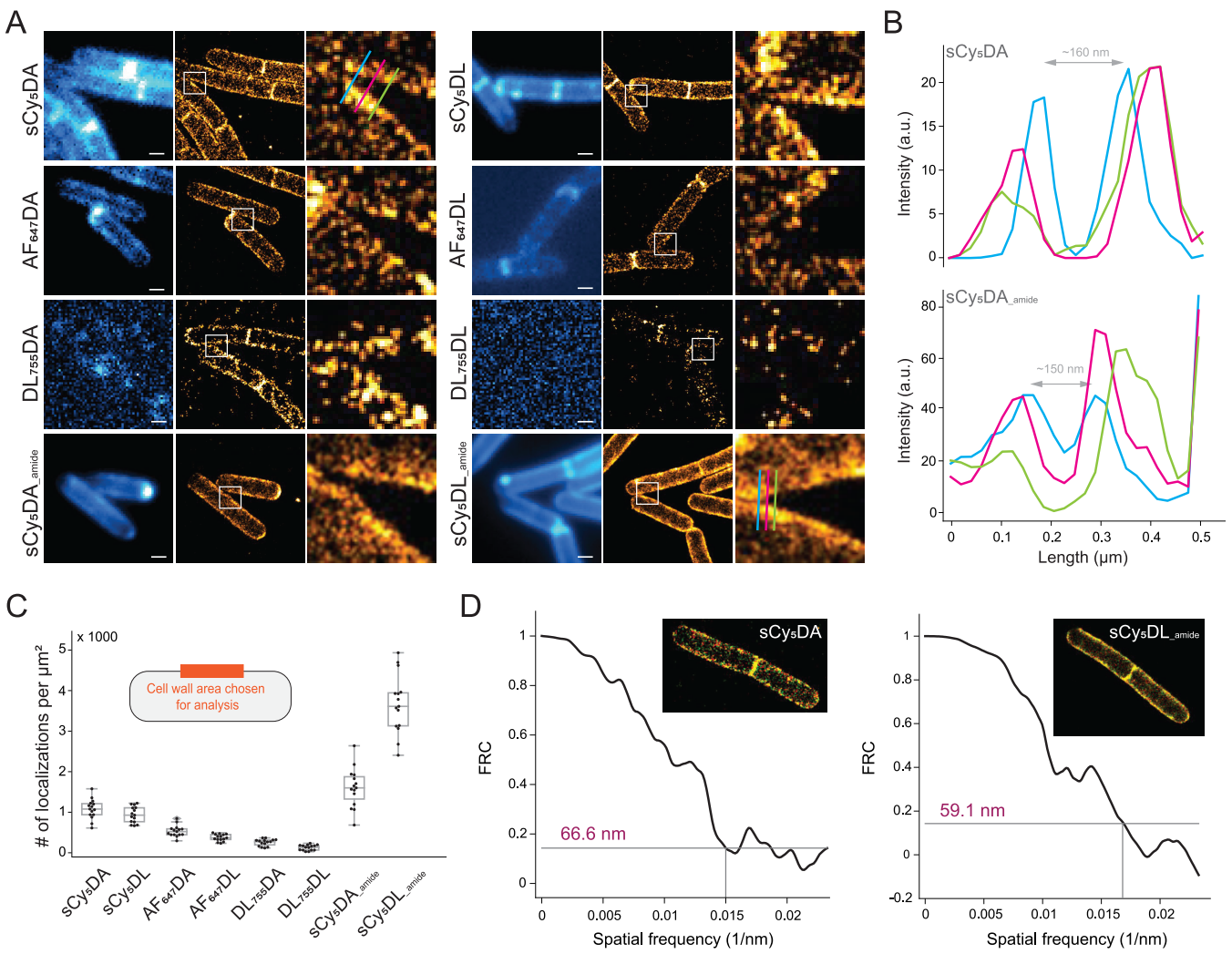

Figure 2. (A) WF (left), SMLM (middle) and zoom-in SMLM (right) images of *B. subtilis* cells labeled with FDAAs. Cell-cell contact areas highlighted. Scale bar: 1 μm. (B) Intensity profiles for three lines drawn in zoomed image in (A), profile color corresponds to line color in (A). (C) Localization density measured in cell wall region (insert schematic, orange rectangle). N = 15 cells for each FDAA. (D) FRC calculated for SMLM images of sCy_5DA (left) and $sCy_5DL_{\_amide}$ (right) labeled cells (Supplementary Methods).

https://doi.org/10.1021/acschembio.2c00496
ACS Chem. Biol. 2022, 17, 2418–2424

alanine (Cy_3BADA) were synthesized and tested for photoblinking and SMLM imaging.[4] Although the dyes incorporated well into *Escherichia coli* cells, SMLM revealed patchy images of the cell envelope, where the poles and septum were missing. This suggests that TDL and Cy_3BADA are able to penetrate the cell wall and cross-link with PG, but they are not suitable dyes for SMLM imaging. In the second case, click reactions were applied to link Alexa-Fluor 647 (AF_{647}) to DAA derivatives after their incorporation into the cell wall. Subsequent SMLM imaging offered nanoscale PG visualization in *Staphylococcus aureus* and *Streptococcus pneumoniae* cells,[11,12] although with the inconvenience of two-step labeling.

We demonstrate a streamlined strategy, for efficient incorporation and photoblinking, while retaining the simplicity of single-step labeling. We discovered that the results of this strategy, combining dyes known to be optimal for SMLM with different DAA backbones, can be optimized for cell wall incorporation and super-resolution imaging. Here, we report a new set of FDAAs for cell wall labeling, with superior performance for SMLM imaging.

We started with three commercially available fluorophores that have been reported to show high performance in SMLM imaging: Sulfo-Cyanine 5 (sCy_5), Alexa Fluor 647 (AF_{647}), and DyLight 755 (DL_{755}).[13,14] Following a chemical synthesis method similar to the one previously reported[1] (Supplementary Methods), we conjugated these fluorophores to D-alanine (DA) and D-lysine (DL) backbones, respectively, to make new FDAAs: sCy_5DA, sCy_5DL, AF_{647}DA, AF_{647}DL, DL_{755}DA, and DL_{755}DL (Figures 1A−C, S1−S6). Additionally, we made sCy5DA$_{_amide}$ and sCy5DL$_{_amide}$, the amide versions of sCy_5DA and sCy_5DL, respectively (Figures 1D, S7, S8). Such amide-modified FDAA derivatives were reported to be better incorporated into the cell wall of many Gram-positive bacteria, compared with carboxyl group-containing FDAAs.[15]

We next tested the dye incorporation by incubating these new FDAAs with *Bacillus subtilis* cell cultures for ∼1 cell cycle during exponential growth phase. The Gram-positive *B. subtilis* lacks an outer membrane; thus, the cell wall is readily accessible to probes in the growth media. In widefield (WF) images, cells labeled with either sCy_5 or AF_{647} derivatives showed a clear cell outline where the cell periphery and septum could be distinctly observed (Figures 1E,F, S9). In contrast, cells incubated with DL_{755} derivatives appeared decorated with small blobs of dye and yielded low contrast images, where cell shape details could barely be inferred (Figures 1G, S10). This indicated that the DL_{755} derivatives suffered from poor cell wall incorporation. The molecular weight of DL_{755} (1092 g/mol, NHS ester) is intermediate to those of sCy_5 (778 g/mol, NHS ester) and AF_{647} (1250 g/mol, NHS ester), indicating that size is probably not the issue. While the formula of DL_{755} has not been disclosed, we suspect that the chemical properties of DL_{755} (e.g., net charge, hydrophobicity) may inhibit its cell wall incorporation and thus limit its labeling efficiency. WF images of sCy5DA$_{_amide}$ and sCy5DL$_{_amide}$ labeled *B. subtilis* cells (Figures 1H, S11) also showed clear outlines and septum similar to sCy_5DA and sCy_5DL (Figure 1E).

We then performed SMLM imaging of *B. subtilis* cells labeled with each of the eight new FDAAs. As desired, the cell outline and septum are clearly apparent in reconstructed SMLM images, except for those cells labeled with DL_{755}DL and DL_{755}DA (Figures 2A, S10). We also tested SMLM imaging of TDL-labeled *B. subtilis* under the same experimental conditions (Figures S13, S14). Here, the overall bacterial shape (e.g., cell pole and septum) observed in WF could barely be detected by SMLM. Both DL_{755} derivatives and TDL were incompatible with high quality SMLM imaging, but for different reasons: DL_{755} fails to incorporate, while TDL fails to photoblink. For the other FDAAs, we used regions of close proximity between two cells to examine image quality. Cells labeled with sCy_5DA, sCy_5DA$_{_amide}$, sCy_5DL, sCy_5DL$_{_amide}$, and AF_{647}DA demonstrated a clear "V-shape" pattern with continuous cell wall localizations, while those labeled with AF_{647}DL appeared slightly patchy (Figure 2A). The distance between distinguishable features reflects the image quality, so we quantified the distance between adjacent cell walls with line profiles. For sCy_5DA- and sCy_5DL$_{_amide}$-labeled cells, we found neighboring cells could be resolved at ∼150 nm apart (Figure 2B).

SMLM images are pointillist reconstructions of molecular positions; thus, their quality depends in part on the density of localized molecules. We compared the mean density of localizations in the lateral cell wall. Among the six acid version FDAAs, sCy_5 was the best-performing fluorophore (∼1000 loc/μm^2) followed by AF_{647} (∼500 loc/μm^2) and DL_{755} (∼200 loc/μm^2) (Figure 2C). Since AF_{647} was reported to exhibit the best photophysical properties for SMLM,[13] the higher sCy_5 localization density could be due to better cell wall incorporation. With a net charge of −1, sCy_5 should be more readily incorporated into the also negatively charged cell wall, compared to AF_{647} with its net charge of −3.[16] This is consistent with the lower intensity of WF images collected under identical imaging conditions (Figure 1E,F). Overall, the amidated sCy_5DL$_{_amide}$ (∼4000 loc/μm^2) and sCy_5DA$_{_amide}$ (∼2000 loc/μm^2) enabled the highest localization densities. Labeling density is a consequence of retention as well as incorporation: sCy_5DA$_{_amide}$ and sCy_5DL$_{_amide}$ are charge neutral, and amidation of the stem peptides may confer resistance against transpeptidase-mediated displacement.[15] Since sCy_5DA$_{_amide}$ resulted in a lower labeling density than sCy_5DL$_{_amide}$, *B. subtilis* transpeptidases may catalyze D-alanine based carboxamides more efficiently.

Finally, we used the Fourier ring correlation (FRC) method to measure the image resolution. FRC measures the correlation between two images−reconstructed from subsets of the localizations−at different spatial frequencies, thus providing an estimation of SMLM image resolution.[17] It is indirectly sensitive to different factors, including the localization uncertainty, labeling density, and the sample's spatial structure. For cells labeled with sCy_5DA and sCy_5DL$_{_amide}$, the calculated FRC resolution was ∼60 nm (Figure 2D). Calculated for different images, the FRC resolution ranged between 50 and 110 nm, with similar results obtained for sCy_5DA, sCy_5DA$_{_amide}$, sCy_5DL, sCy_5DL$_{_amide}$, and AF_{647}DA labeling (Figure S15). The calculation of FRC resolutions for SMLM images of DL_{755}DA, DL_{755}DL, and TDL labeled cells failed, consistent with our conclusion that these dyes are not reliable for SMLM imaging. Overall, sCy_5DL$_{_amide}$ performed best as an FDAA for SMLM imaging of *B. subtilis*, with sCy_5DA$_{_amide}$, sCy_5DA, sCy_5DL, and AF_{647}DA being good alternatives.

We next applied SMLM imaging to resolve nascent PG growth in *Caulobacter crescentus*. We chose *C. crescentus* as a challenging case, due to its small size (∼500 nm in diameter) and the fact that it is Gram-negative, with an outer cell membrane that could act as a permeability barrier to our probes. We found sCy_5DA to be a better label for *C. crescentus* than sCy_5DL$_{_amide}$ (Figure S16), consistent with a previous

https://doi.org/10.1021/acschembio.2c00496
ACS Chem. Biol. 2022, 17, 2418−2424

study that reported Gram-negative bacteria incorporated D-amino carboxamides less effectively.[15] *C. crescentus* has a well-characterized PG growth model: dispersed insertion along the sidewalls during elongation, asymmetric growth between the lateral sides to give rise to cell curvature,[18,19] polar PG remodeling during stalk formation,[20] and then zonal insertion at midcell prior to division and during constriction.[21] To highlight newly synthesized PG, we performed pulse-chase labeling where cells were incubated with a green FDAA (sBADA) for more than one generation, followed by a short-pulse labeling with sCy_5DA for only 5 min (~5% of cell cycle duration) (Figure 3A).

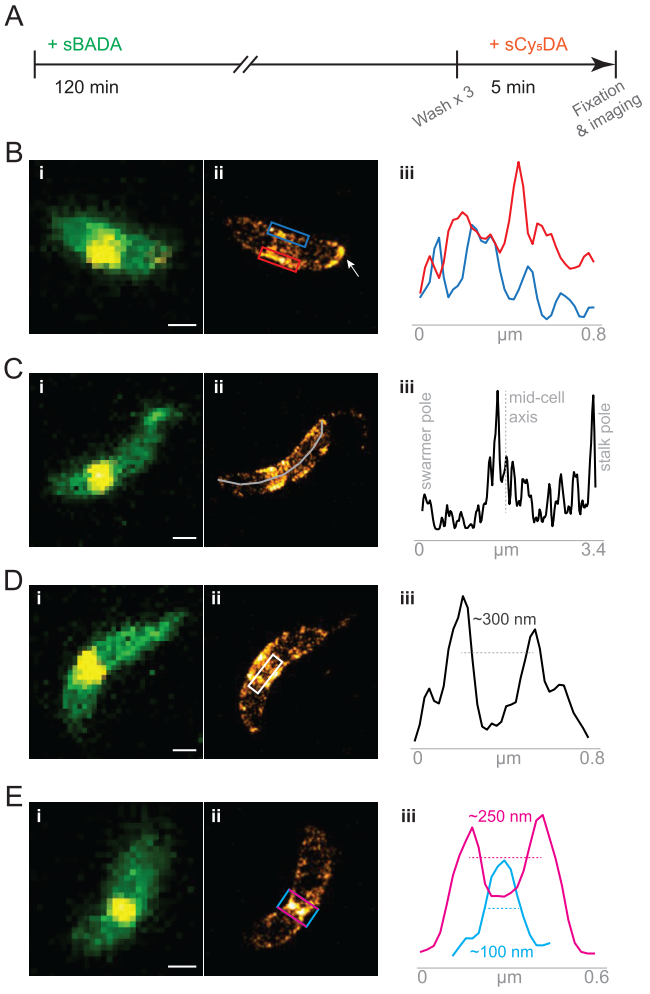

Figure 3. (A) Schematic of the pulse-chase labeling strategy: *C. crescentus* cultured in PYE was incubated with 0.25 mM sBADA for 120 min, then with 0.5 mM sCy_5DA for 5 min. (B–E) (i) WF images of pulse-chase labeled *C. crescentus* cells, sBADA (green) and sCy_5DA (yellow); (ii) SMLM imaging of sCy_5DA; (iii) intensity profile along the long axis of rectangle (B and D), the midline (C), or two axes of the rectangle (E). Scale bar: 500 nm.

We examined the organization of PG synthesis in *C. crescentus* cells at different stages of the cell cycle (Figures 3B–E, S17). In some cases (Figure 3B), both visual examination and intensity profile showed higher labeling of one lateral cell wall (red box), compared with the other (blue box). This is consistent with the overall cell curvature, where PG insertion into the outer (convex) wall is enhanced relative to the inner (concave) wall. Polar PG insertion (white arrow) is also visible at one cell end, perhaps indicating the onset of stalk growth. We observed PG insertion along the longitudinal cell axis to be asymmetric relative to midcell, with the stalked pole showing higher PG remodeling than the flagellar pole (Figure 3C). We also noticed that the zonal PG band at midcell was slightly shifted toward the flagellar pole. We observed a few cells (Figures 3D, S18) with an unusual double-ring of PG insertion at midcell rather than the more common single band (Figure 3B). Zonal PG growth in *C. crescentus* occurs during both cell elongation and division, shifting from more dispersed to more constrained at the division site during septum formation. The double-band structure here might indicate a transition state during cell constriction. Notably, the bacterial septal PG growth is driven by the FtsZ-containing protein complex called the divisome, and in *Streptococcus pneumoniae* FtsZ can form a double-ring.[22] In a predivisional cell (Figure 3E), we found that the septal PG appeared as a ring-like band with a small nonlabeled region at the center. Such a dip in intensity could result from a 2D projection of the septal PG ring. The intensity profile along two orthogonal directions (blue, along the cell length and red, along the cell width) showed a septal width of ~100 nm, while the distance between two lateral PG peaks was ~250 nm.

Since $sCy_5DL_{\_amide}$ incorporated well into Gram-positive *B. subtilis* while sCy_5DA was superior for Gram-negative *C. crescentus* cells, we next examined the labeling in other bacterial species using the two dyes. We focused on human pathogens, where fundamental knowledge of their PG growth characteristics is of particular interest. We performed a long-pulse labeling (1–2 cell cycle durations) of 12 different species and assessed cell wall incorporation as well as the quality of the corresponding SMLM images.

Gram-negative bacteria generally retained less fluorescence compared to Gram-positive and mycobacteria. We therefore used a higher dye concentration for their labeling. Among them, *Pseudomonas aeruginosa* showed cell-to-cell variation of labeling density, compared to the more homogeneous staining in *C. crescentus*, *Vibrio cholerae*, or *Klebsiella pneumoniae* bacteria (Figures 4A, S19). The weak labeling of *P. aeruginosa* could result from its thin PG sacculus (~3 nm) compared to that of *E. coli* (~6 nm) and *C. crescentus* (~7 nm),[23−25] and low permeability of its outer membrane.[26] The Gram-positive bacteria showed more continuous and denser labeling either with $sCy_5DL_{\_amide}$ or sCy_5DA, with the septum of *B. subtilis* and *Paraclostridium*, the equatorial ring of *Staphylococcus aureus*, and the size variance of *Streptococcus pneumoniae* cells all clearly visible in SMLM images (Figures 4B, S19).

Mycobacteria are different from Gram-negative and -positive bacteria due to their unique cell wall architecture which includes a waxy surface layer composed of long-chain fatty acids, mycolic acids.[27] SMLM images of *M. smegmatis*, *M. abssensus*, and *M. marinum* revealed details lacking from WF images, such as a rough cell surface whose width varies along the mostly cylindrical cell wall (Figures 4C, S20). We found that *M. tuberculosis* easily forms aggregates during cultivation, which may lead to nonuniform labeling in SMLM images. Nevertheless, isolated *M. tuberculosis* cells were well-labeled and highly resolved (Figures 4C, S20). We further tested short-pulse labeling of *M. smegmatis* for ~10% of cell cycle duration. Consistent with previous reports that asymmetric division in *M. smegmatis* results from differential growth at the cell tips,[28] we observed an asymmetry between the PG inserted into the two cell poles (Figures S21, S22). Interestingly, we also

https://doi.org/10.1021/acschembio.2c00496
ACS Chem. Biol. 2022, 17, 2418−2424

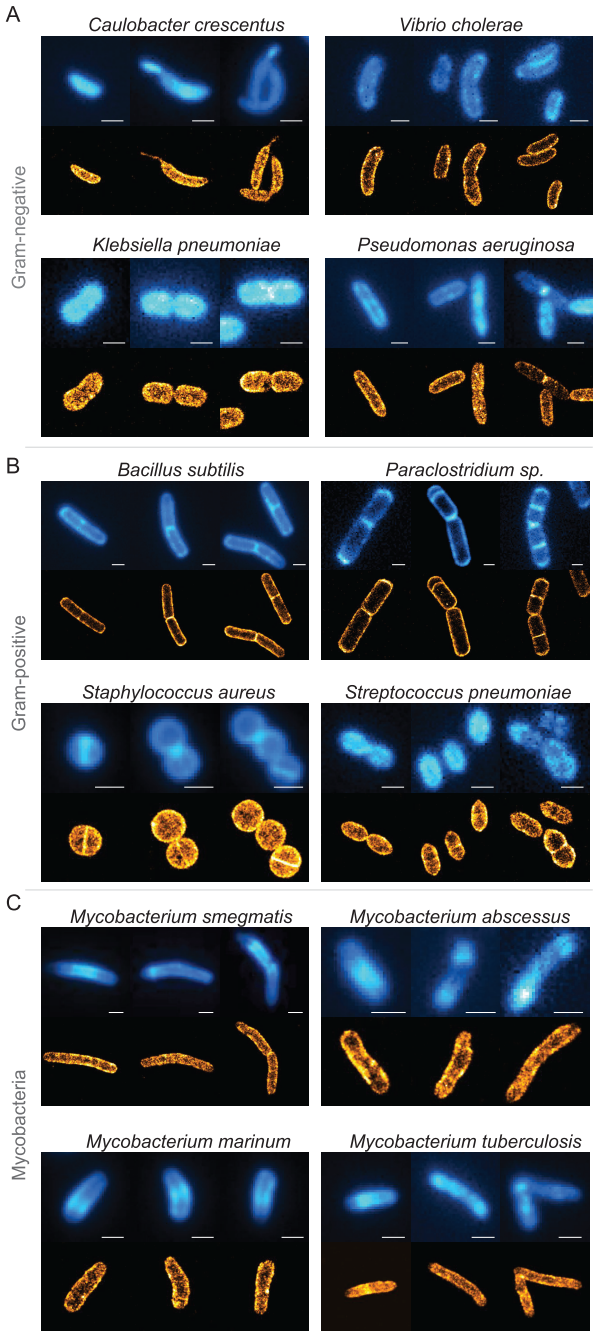

Figure 4. WF and SMLM imaging of (A) Gram-negative bacteria: *C. crescentus* (0.5 mM sCy_5DA), *V. cholerae* (0.5 mM sCy_5DA), *K. pneumoniae* (0.5 mM sCy_5DA), *P. aeruginosa* (1 mM sCy_5DA), (B) Gram-positive bacteria: *B. subtilis* (0.1 mM sCy_5DL_{amide}), *Paraclostridium* spp. (0.1 mM sCy_5DA), *S. aureus* (0.1 mM sCy_5DA), *S. pneumoniae* (0.1 mM sCy_5DA), and (C) mycobacteria: *M. smegmatis* (0.1 mM sCy_5DA), *M. abscessus* (0.5 mM sCy_5DA), *M. marinum* (1 mM sCy_5DL_{amide}), *M. tuberculosis* (1 mM sCy_5DL_{amide}). Scale bar: 1 μm.

observed cells in which the nascent PG was concentrated at one pole and dispersed on the other cell half, which lacked polar growth. This is compatible with a previous atomic force microscopy (AFM) study, which proposed a biphasic growth model in which the new cell pole experiences a lag when switching from a slow to fast growth mode initiated by the old pole.[29]

The FDAAs reported here incorporate well to highlight the cell wall in a wide variety of bacteria, including Gram-positive, Gram-negative, and mycobacteria. The dyes sCy_5DA, sCy_5DA_{amide}, sCy_5DL, sCy_5DL_{amide}, and $AF_{647}DA$ outperformed other probes for SMLM applications with good incorporation and photoblinking capabilities. When used for SMLM imaging, they can reveal details of cell shape and PG distribution lacking from standard WF imaging. Combined with spectrally distinct protein markers, they can enable multicolor super-resolution studies of cell growth. In experimental designs using pulse-labeling, our new probes can advance the study of bacterial cell wall organization with unprecedented spatial detail.

■ ASSOCIATED CONTENT

Supporting Information

The Supporting Information is available free of charge at https://pubs.acs.org/doi/10.1021/acschembio.2c00496.

Materials, instrumentation, experimental methods and procedures, image processing and analysis methods, liquid chromatography data, and additional image examples (PDF)

■ AUTHOR INFORMATION

Corresponding Author

Suliana Manley − *Institute of Physics, School of Basic Sciences, Swiss Federal Institute of Technology Lausanne (EPFL), Lausanne 1015, Switzerland;* orcid.org/0000-0002-4755-4778; Email: suliana.manley@epfl.ch

Authors

Chen Zhang − *Institute of Physics, School of Basic Sciences, Swiss Federal Institute of Technology Lausanne (EPFL), Lausanne 1015, Switzerland;* orcid.org/0000-0003-1468-2906

Luc Reymond − *Biomolecular Screening Core Facility, Swiss Federal Institute of Technology Lausanne (EPFL), Lausanne 1015, Switzerland*

Ophélie Rutschmann − *Global Health Institute, School of Life Sciences, Swiss Federal Institute of Technology Lausanne (EPFL), Lausanne 1015, Switzerland*

Mischa A. Meyer − *Institute of Physics, School of Basic Sciences and Global Health Institute, School of Life Sciences, Swiss Federal Institute of Technology Lausanne (EPFL), Lausanne 1015, Switzerland;* orcid.org/0000-0002-5336-4647

Julien Denereaz − *Department of Fundamental Microbiology, Faculty of Biology and Medicine, University of Lausanne (UNIL), Lausanne 1015, Switzerland*

Jiangtao Qiao − *Environmental Engineering Institute, School of Architecture, Civil and Environmental Engineering, Swiss Federal Institute of Technology Lausanne (EPFL), Lausanne 1015, Switzerland*

Faustine Ryckebusch − *Global Health Institute, School of Life Sciences, Swiss Federal Institute of Technology Lausanne (EPFL), Lausanne 1015, Switzerland*

Juliette Griffié − *Institute of Physics, School of Basic Sciences, Swiss Federal Institute of Technology Lausanne (EPFL), Lausanne 1015, Switzerland*

Willi L. Stepp − *Institute of Physics, School of Basic Sciences, Swiss Federal Institute of Technology Lausanne (EPFL), Lausanne 1015, Switzerland*

Complete contact information is available at:
https://pubs.acs.org/10.1021/acschembio.2c00496

Author Contributions

C.Z., L.R. and S.M. conceived and designed the project. C.Z. and S.M. supervised the project. C.Z. performed the SMLM imaging experiments and analysis. L.R. synthesized and characterized the new dyes. O.R. prepared mycobacteria samples; M.M. prepared *V. cholerae*, *K. pneumoniae*, and *P. aeruginosa* samples; J.D. prepared *S. pneumoniae* samples; J.Q. prepared *Paraclostridium sp*. samples; F.R. prepared *S. aureus* samples. J.G. validated SMLM analysis and discussed results, W.S. maintained the microscope and discussed results. C.Z. and S.M. wrote the manuscript with contributions from all authors.

Funding

This work was supported in part by the National Centre of Competence in Research Chemical Biology (L.R., S.M.), the EPFL-SV iPhD Program (M.A.M.), the Swiss National Science Foundation (182429, W.L.S.), and the European Union's H2020 program under the Marie Skłodowska-Curie Fellowships (BALTIC, J.G.) and ERC Consolidator Grants (Piko, S.M.).

Notes

The authors declare no competing financial interest.

■ ACKNOWLEDGMENTS

We thank H. Antar from S. Gruber lab (UNIL) for the gift of the *B. subtilis* strain, and C. Sieben (HZI) for maintaining the microscope and testing our new FDAA probes. We also thank L. Bianchi for work on optimizing the imaging protocol of *M. smegmatis*.

■ REFERENCES

(1) Kuru, E.; Hughes, H. V.; Brown, P. J.; Hall, E.; Tekkam, S.; Cava, F.; de Pedro, M. A.; Brun, Y. V.; VanNieuwenhze, M. S. In Situ Probing of Newly Synthesized Peptidoglycan in Live Bacteria with Fluorescent D-Amino Acids. *Angew. Chem.* **2012**, *124* (50), 12687−12691.

(2) Kuru, E.; Tekkam, S.; Hall, E.; Brun, Y. V.; Van Nieuwenhze, M. S. Synthesis of Fluorescent D-Amino Acids and Their Use for Probing Peptidoglycan Synthesis and Bacterial Growth in Situ. *Nat. Protoc.* **2015**, *10* (1), 33−52.

(3) Kuru, E.; Radkov, A.; Meng, X.; Egan, A.; Alvarez, L.; Dowson, A.; Booher, G.; Breukink, E.; Roper, D. I.; Cava, F.; et al. Mechanisms of Incorporation for D-Amino Acid Probes That Target Peptidoglycan Biosynthesis. *ACS Chem. Biol.* **2019**, *14* (12), 2745−2756.

(4) Hsu, Y.-P.; Rittichier, J.; Kuru, E.; Yablonowski, J.; Pasciak, E.; Tekkam, S.; Hall, E.; Murphy, B.; Lee, T. K.; Garner, E. C.; et al. Full Color Palette of Fluorescent D-Amino Acids for in Situ Labeling of Bacterial Cell Walls. *Chem. Sci.* **2017**, *8* (9), 6313−6321.

(5) Hsu, Y.-P.; Hall, E.; Booher, G.; Murphy, B.; Radkov, A. D.; Yablonowski, J.; Mulcahey, C.; Alvarez, L.; Cava, F.; Brun, Y. V.; et al. Fluorogenic D-Amino Acids Enable Real-Time Monitoring of Peptidoglycan Biosynthesis and High-Throughput Transpeptidation Assays. *Nat. Chem.* **2019**, *11* (4), 335−341.

(6) Huang, B.; Bates, M.; Zhuang, X. Super-Resolution Fluorescence Microscopy. *Annu. Rev. Biochem.* **2009**, *78* (1), 993−1016.

(7) Kuru, E.; Lambert, C.; Rittichier, J.; Till, R.; Ducret, A.; Derouaux, A.; Gray, J.; Biboy, J.; Vollmer, W.; VanNieuwenhze, M. S.; et al. Fluorescent D-Amino-Acids Reveal Bi-Cellular Cell Wall Modifications Important for *Bdellovibrio bacteriovorus* Predation. *Nat. Microbiol.* **2017**, *2* (12), 1648−1657.

(8) Bisson-Filho, A. W.; Hsu, Y.-P.; Squyres, G. R.; Kuru, E.; Wu, F.; Jukes, C.; Sun, Y.; Dekker, C.; Holden, S.; VanNieuwenhze, M. S.; et al. Treadmilling by FtsZ Filaments Drives Peptidoglycan Synthesis and Bacterial Cell Division. *Science* **2017**, *355* (6326), 739−743.

(9) Hsu, Y.-P.; Booher, G.; Egan, A.; Vollmer, W.; VanNieuwenhze, M. S. D-Amino Acid Derivatives as in Situ Probes for Visualizing Bacterial Peptidoglycan Biosynthesis. *Acc. Chem. Res.* **2019**, *52* (9), 2713−2722.

(10) Rust, M. J.; Bates, M.; Zhuang, X. Sub-Diffraction-Limit Imaging by Stochastic Optical Reconstruction Microscopy (STORM). *Nat. Methods* **2006**, *3* (10), 793−796.

(11) Lund, V. A.; Wacnik, K.; Turner, R. D.; Cotterell, B. E.; Walther, C. G.; Fenn, S. J.; Grein, F.; Wollman, A. J.; Leake, M. C.; Olivier, N.; et al. Molecular Coordination of *Staphylococcus aureus* Cell Division. *eLife* **2018**, *7*, No. e32057.

(12) Trouve, J.; Zapun, A.; Arthaud, C.; Durmort, C.; Di Guilmi, A. M.; Söderström, B.; Pelletier, A.; Grangeasse, C.; Bourgeois, D.; Wong, Y.-S. Nanoscale Dynamics of Peptidoglycan Assembly during the Cell Cycle of *Streptococcus pneumoniae*. *Curr. Biol.* **2021**, *31*, 2844.

(13) Dempsey, G. T.; Vaughan, J. C.; Chen, K. H.; Bates, M.; Zhuang, X. Evaluation of Fluorophores for Optimal Performance in Localization-Based Super-Resolution Imaging. *Nat. Methods* **2011**, *8* (12), 1027−1036.

(14) Sieben, C.; Banterle, N.; Douglass, K. M.; Gönczy, P.; Manley, S. Multicolor Single-Particle Reconstruction of Protein Complexes. *Nat. Methods* **2018**, *15* (10), 777−780.

(15) Pidgeon, S. E.; Fura, J. M.; Leon, W.; Birabaharan, M.; Vezenov, D.; Pires, M. M. Metabolic Profiling of Bacteria by Unnatural C-Terminated D-Amino Acids. *Angew. Chem.* **2015**, *127* (21), 6256−6260.

(16) Hurst, L. *Bacteriology*; EDTECH, 2019.

(17) Nieuwenhuizen, R. P. J.; Lidke, K. A.; Bates, M.; Puig, D. L.; Grünwald, D.; Stallinga, S.; Rieger, B. Measuring Image Resolution in Optical Nanoscopy. *Nat. Methods* **2013**, *10* (6), 557−562.

(18) Ausmees, N.; Kuhn, J. R.; Jacobs-Wagner, C. The Bacterial Cytoskeleton: An Intermediate Filament-Like Function in Cell Shape. *Cell* **2003**, *115* (6), 705−713.

(19) Surovtsev, I. V.; Jacobs-Wagner, C. Subcellular Organization: A Critical Feature of Bacterial Cell Replication. *Cell* **2018**, *172* (6), 1271−1293.

(20) Kühn, J.; Briegel, A.; Mörschel, E.; Kahnt, J.; Leser, K.; Wick, S.; Jensen, G. J.; Thanbichler, M. Bactofilins, a Ubiquitous Class of Cytoskeletal Proteins Mediating Polar Localization of a Cell Wall Synthase in *Caulobacter crescentus*. *EMBO J.* **2010**, *29* (2), 327−339.

(21) Aaron, M.; Charbon, G.; Lam, H.; Schwarz, H.; Vollmer, W.; Jacobs-Wagner, C. The Tubulin Homologue FtsZ Contributes to Cell Elongation by Guiding Cell Wall Precursor Synthesis in *Caulobacter crescentus*. *Mol. Microbiol.* **2007**, *64* (4), 938−952.

(22) Jacq, M.; Adam, V.; Bourgeois, D.; Moriscot, C.; Di Guilmi, A.-M.; Vernet, T.; Morlot, C. Remodeling of the Z-Ring Nanostructure during the *Streptococcus pneumoniae* Cell Cycle Revealed by Photoactivated Localization Microscopy. *mBio* **2015**, *6* (4), e01108-15.

(23) Gan, L.; Chen, S.; Jensen, G. J. Molecular Organization of Gram-Negative Peptidoglycan. *Proc. Natl. Acad. Sci. U. S. A* **2008**, *105* (48), 18953−18957.

(24) Goley, E. D.; Comolli, L. R.; Fero, K. E.; Downing, K. H.; Shapiro, L. DipM Links Peptidoglycan Remodelling to Outer Membrane Organization in Caulobacter. *Mol. Microbiol.* **2010**, *77* (1), 56−73.

(25) Vollmer, W.; Seligman, S. J. Architecture of Peptidoglycan: More Data and More Models. *Trends Microbiol.* **2010**, *18* (2), 59−66.

(26) Yoshimura, F.; Nikaido, H. Permeability of *Pseudomonas aeruginosa* Outer Membrane to Hydrophilic Solutes. *J. Bacteriol.* **1982**, *152* (2), 636−642.

(27) Chiaradia, L.; Lefebvre, C.; Parra, J.; Marcoux, J.; Burlet-Schiltz, O.; Etienne, G.; Tropis, M.; Daffé, M. Dissecting the Mycobacterial Cell Envelope and Defining the Composition of the Native Mycomembrane. *Sci. Rep.* **2017**, *7* (1), 12807.

(28) Joyce, G.; Williams, K. J.; Robb, M.; Noens, E.; Tizzano, B.; Shahrezaei, V.; Robertson, B. D. Cell Division Site Placement and

Asymmetric Growth in Mycobacteria. *PLoS One* **2012**, *7* (9), No. e44582.
(29) Hannebelle, M. T. M.; Ven, J. X. Y.; Toniolo, C.; Eskandarian, H. A.; Vuaridel-Thurre, G.; McKinney, J. D.; Fantner, G. E. A Biphasic Growth Model for Cell Pole Elongation in Mycobacteria. *Nat. Commun.* **2020**, *11* (1), 1−10.

https://doi.org/10.1021/acschembio.2c00496
ACS Chem. Biol. 2022, 17, 2418−2424